View metadata, citation and similar papers at core.ac.uk

brought to you by CORE

provided by Directory of Open Access Journals

Journal of Applied Fluid Mechanics, Vol. 12, No. 5, pp. 1683-1696, 2019.
Available online at www.jafmonline.net, ISSN 1735-3572, EISSN 1735-3645.
DOI: 10.29252/jafm.12.05.29553

Effect of Different S AC Based Nanoparticles Types on the Reflow Soldering Process of Miniaturized Component using Discrete Phase Model Simulation

M. A. Fatah M. Mukhtar[1], A. Abas[2†], M. S. Haslinda[2], F. Che Ani[3, 4], A. Jalar[3], A. A. Saad[2], M. Z. Abdullah[5] and R. Ismail[3]

[1] *Faculty of Engineering, DRB-HICOM University of Automotive Malaysia, 26607 Pekan, Pahang, Malaysia*
[2] *School of Mechanical Engineering, Universiti Sains Malaysia, Engineering Campus, 14300 Nibong Tebal, Penang, Malaysia*
[3] *Institute of Microengineering and Nanoelectronics, Universiti Kebangsaan Malaysia, 43600 Bangi, Selangor, Malaysia*
[4] *Jabil Circuits, 56, Hilir Sungai Kluang 1, Bayan Lepas, 11900 Penang, Malaysia*
[5] *School of Aerospace Engineering, Universiti Sains Malaysia, Engineering Campus, 14300 Nibong Tebal, Penang, Malaysia*

†*Corresponding Author Email: aizatabas@usm.my*

(Received August 20, 2018; accepted December 26, 2018)

ABSTRACT

The wetting formation and nanoparticles dispersion on adding nanoparticles to the lead free solder Sn-3.0Ag-0.5Cu (SAC305) is methodically investigated using Discrete Phase Model (DPM) simulation and applied on a 01005 capacitor component. Different types of nanoparticles, namely titanium dioxide (TiO_2), nickle oxide (NiO) and Iron (III) oxide (Fe_2O_3) with varying weight percentages, 0.01wt%, 0.05wt% and 0.15wt% that is doped in SAC305 are used. The study of two-way interactions between multiphase volume of fluid (VOF) and discrete phase model (DPM) shows excellent capability in tracking the dispersed nanoparticles immersed in the wetted molten solder. In this study, real reflow profile temperature setup will be used to mimic the conventional reflow process. Based on the findings, the fillet height managed to achieve the minimum required height set by IPC standards. As the concentration of the nanoparticles doped in the molten solder increases, higher time is required for the wetting process. In general, the doped NiO nanoparticles at 0.05wt% has the lowest wetting time compared to other cases. The study of the instantaneous nanoparticles trajectory tracking was also conducted on a 3D model and 2D cross sectional view to identify the exact movement of the particles. Additionally, it was also observed that the velocity and pressure distribution increases as the weight percentage of the nanoparticles increases.

Keywords: Nanoparticle; SAC305; Numerical simulation; Discrete phase model; Nanocomposite solder paste.

NOMENCLATURE

Nomenclature should be in alphabetic order (A – Z) and Greek letters should follow after Latin letters in alphabetic *order (α β ...)*

C_c	cunningham factor	K	constant, 2.594
C_D	drag coefficient	n	particle number
C_p	specific heat	P	pressure
d_{ij}, d_{ik}, d_{kj}	deformation tensor	Re	Reynold number
D_T	thermophoric coefficient	S_P	Surface area
f	fluid volume fraction	V_p	Volume
F_B	brownian force	T	temperature
F_D	drag force	t	time
F_L	saffman's lift force	u, v, w	velocity
g	gravity		
h	height	ρ	density
k	thermal conductivity	μ	viscosity

Φ	polar coordinate
$\bar{\bar{\tau}}$	shear stress
σ	surface tension coefficient
θ	contact angle
λ	Particle's mean free path
ψ	Particle sphericity
ϕ	shape factor
ξ	zero mean

1. INTRODUCTION

The requirement placed for high reliability electronic components, miniaturization of the active and passive components are forcing engineers and designers to further optimize the existing manufacturing method. Current, the electronic industries are pushing towards higher performance device with emphasis also on miniaturization of the components. The addition of nanoreinforced material on the lead free solder has become an impending method in order to enhance the reliability and performance of the solder joint at micro- and nano- scales level (Lee *et al.*, 2005). Guo (2017) introduce the effect of the reinforcement addition on the mechanical properties of the composite lead free solder with the experimental result indicating significant improvement on the reliability of the nanocomposite solder joint. Liu *et al.* (2016) conducted a study on the microstructure transformation as result of increment in the doped nanoparticles with the hardness and the elastic modulus of the solder joint found to be reduced. It has been well known that lead free solder, especially Sn–Ag–Cu; SAC solder is becoming the common solder paste used in electronic packaging industry Previous study on lead solder, Sn-Pb, especially on the thermal, mechanical and intermetallic compound (IMC) growth, has led to the subsequent interest on the incorporation of nano-reinforced lead solder in an attempt to further increase the reliability of the solder joint. Various types of reinforced material has been studied and doped into the lead free solder in order to enhance its reliability with materials such as Ni, Co, Fe, In, Zn, Sb and Billah *et al.* (2012) studied on the addition of micron-sized Ni as the reinforced material to the composite solder, with different percentages of reinforced material introduced to improve the mechanical properties of the tensile strength and hardness of the composite solder. While, Fallahi *et al.* (2012) pointed out the effect of Fe and In on the IMC formation and mechanical properties of the nano-reinforced lead free solder. It was found that the wettability and the shear strength improved by the introduction of this reinforced material. Additionally, the ductility of the solder joint with the interface had increased. Other materials have also being used as reinforced material. In a study by Lee *et al.* (2008) that focuses on the use of Co as reinforced material in the lead free solder has found that Co addition managed to increase the shear strength by 28% due to the additional reinforcing force. These reinforcement elements have impact on the properties of the solder such as improved mechanical strength, reduction in microstructure interfacial intermetallic compounds (IMCs) creation and to improve the solidification process (Kotadia *et al.*, 2014). The addition of nano-reinforced material to the lead free solder has been conducted by few researchers. Chellvarajoo and Abdullah (2016) conducted the study on the microstructure and mechanical properties of the SAC305 with NiO nanoparticles. The study shows that the nanocomposite lead free solder can significantly reduce the intermetallic compound (IMC) and improved the hardness by 50% (Chellvarajoo and Abdullah, 2016). In another study conducted by Chellvarajoo *et al.* (2015), the addition of diamond nanoparticles at 0.05wt% increased the hardness by 77.5% and mixing of 0.5, 1.5, and 2.5 wt.% of Fe_2NiO_4 nanoparticles in SAC305 also hinder the excessive growth of IMC layer on the solder joint (Chellvarajoo *et al.* 2014). In a study conducted by Chen and Li (2004) on the kinetic of IMC, the effect of adding Sb to lead free solder can retard the growth of the IMC. Besides, Tang *et al.* (2014) shows the addition of TiO2 nanoparticles into SAC solder can improve the hardness value by up to 34% compared to pure SAC305.

The concern on the intermetallic compound (IMC) growth is becoming more and more crucial in the electronic packaging industry. Most researches conducted previously have shown some correlation between the additions of nano-reinforced particles in solder with the growth of the IMC layer in the solder joint. In the formation of the wetting and fillet also known as solder joint, the formation of Cu-Sn IMC layer will mainly consist of Cu_6Sn_5 and Cu_3Sn. The interface of the IMC layer is crucial in determining the reliability of the component since excessive growth of the IMC layer can be harmful to the functionality of the component (Liu *et al.*, 2016). Salleh *et al.* (2017) conducted further study on the interfacial layer formation that can be suppressed when the nanoparticles are introduced in the lead free solder. The combination of Ni and TiO_2 nanoparticles resulted in improvement of the shear strength. Besides, failure of the solder joint can cause the IMC layer to become fractured thus affecting the mechanical strength of the solder joint (Lee *et al.*, 1999). In the electronics industry, voids in solder joint is considered as a defect that can be influenced by many factors. Various studies concerning on the failure relating to void configuration for electronic packaging have been conducted. Benabou *et al.* (2016) studied void effect to the lead free solder joint at it was found that as the void formation becomes nearer to critical area of the solder joint, significant damage will occur to the connected component. The frequency, location and size of the void that exist in the solder joint is also harmful to the lifetime of the solder joint thus further decreasing the mechanical strength of the solder joint. Ladani and Dasgupta (2007) conducted both experimental and simulation modelling for the durability of the solder joint in which void formation can be detrimental to the reliability of the solder joint. The result of the study also proved the increment in void formation which will affect the

Table 1 Previous research works on reinforcement of solder joint using ceramic nanoparticles added in Pb-free solder paste

Pb-free solder paste (SAC)	Nanoparticles dopant (wt.% of addition)	References
Sn–3.0Ag–0.5Cu	TiO2 (0.02, 0.05, 0.1, 0.3, 0.6, 1.0)	Tang *et al.* (2014) & Gain *et al.* (2011)
	ZrO2 (0.5, 1.0, 3.0)	Gain *et al.* (2011)
	Fe2NiO4 (0.5, 1.5, 2.5)	Chellvarajoo *et al.* (2015)
	Y2O3 (0.1)	Yang *et al.* (2013)
	Trace diamond (0.5, 1.0, 1.5)	Shafiq *et al.* (2013)
	Multi-walled carbon nanotubes (0.01, 0.05, 0.1, 0.5)	Bukat *et al.* (2013)
	Diamond (0.5, 1.5, 2.5)	Chellvarajoo *et al.* (2015)
	TiO2 (0.01, 0.05, 0.15)	Haslinda *et al.* (2017)
Sn–3.5Ag–0.25Cu	TiO2 (0.25, 0.5, 1.0)	Tsao *et al.* (2010)
Sn–3.5Ag–0.5Cu	SrTiO3 (0.5)	Fouzder *et al.* (2011)
	TiO2 (0.25, 0.5, 1.0)	Chang *et al.* (2011) & Chuang *et al.* (2012)
	Al2O3 (0.25, 0.5, 1.0)	Tsao *et al.* (2010) & Tsao *et al.* (2013)
	Multi-walled carbon nanotubes (0.01, 0.05, 0.1)	Xu *et al.* (2014)
	NiO (0.5, 1.5, 2.5)	Chellvarajoo *et al.* (2016)
Sn–3.8Ag–0.7Cu Sn–3.8Ag–0.7Cu	Sb (0, 0.5, 1.0, 1.5)	Chen *et al.* (2004)
	Co (0.5, 1.0, 1.5, 2.0)	Haseeb *et al.* (2011) & Tay *et al.* (2011)
	Mo (1.0, 2.0, 3.0)	Haseeb *et al.* (2012)
	SiC (0.01, 0.05, 0.2)	Liu *et al.* (2008)
	Ni (0.5, 1.0, 1.5, 2.0)	Tay *et al.* (2013)
	Zn (1.0, 2.0)	Chan *et al.* (2013)
Sn-8Zn-3Bi	Ni (0.25, 0.5, 1.0)	Billah *et al.* (2014)

reliability of the joint. Yunus *et al.* (2003) also conducted study on the voids by opting to experimental method with focus on the mechanical failure of the solder joint due to the formation of the void especially at the interface of the solder. The study also found that the void leads to crack that will propagate in the solder joint. This subsequently accelerate the failure of the solder joint.

The study on electronic packaging and solder joint reliability has been frequently conducted using numerical approach such as Finite Element Analysis, Finite Volume Method, Lattice Boltzmann Method and Fluid Structure Interface. Benabou *et al.* (2016) study on the use of Finite Element Analysis for fatigue lifetime of a lead-free solder joint under thermal cycling found that the reliability of the solder joint depends heavily on void configuration. In a study by Abas *et al.* (2015) using Finite Volume Method, the group concerted their effort to study the effect of dispensing types for encapsulation process of electronic packaging applied on different solder bump arrangements. By utilizing a different numerical scheme, Abas *et al.* (2016) applied Lattice Boltzmann Method to observe flow model in a 3D model of BGA for different bump arrangements. Fei Chong *et al.* (2016) also conducted subsequent study on electronic packaging to identify the effect of thermocapillary action on the encapsulation process. The fluid-structure interaction model model used in his study successfully revealed the potential of thermocapillary as the driving force for underfill encapsulation. Specific studies on the application of nanoparticles have previously been conducted using Discrete Phase Method (DPM). The DPM study involves modelling of various sizes and types of discrete particle that was applied on different kind of environments. Ho and Kim (2012) uses DPM model in the study of particle tracking in the water retention, Thiruvengadam *et al.* (2016) also conducted the simulation model on DPM in Ansys Fluent for the study of particulate matter. Similarly, DPM was used in the study conducted by Rashidi *et al.* (2016) for convective AL_2O_3–water nanofluid around a triangular obstacle and Lu *et al.* (2016) which proves the compatibility of DPM model for computer virtual experiment on fluidized beds Based on previous study, the DPM model has been found successful to track the trajectory of the discrete particle in the continuous phase.

Though various experimental studies have been conducted on the reinforced lead free solder, limited studies have been concerted for particles tracking using numerical simulation. Additionally, due to the restriction in micro-level study that includes cost and time consuming experimental method, the need for numerical simulation that be achieved through discrete phase model (DPM) with the capability to track particle trajectory becomes indispensable. In this paper, the tracking of different types of nano-reinforced materials that is doped in the lead free solder at different weight percentages and temperatures will be studied. The interaction of the different types of nanoparticles and the SAC305 molten solder is based on two-way interactions of the continuous-discrete phase simulation. The DPM modelling of the nano-reinforced solder will be applied on real passive component of type 01005 capacitor to mimic the real industrial soldering process.

2. NUMERICAL SIMULATION

The 3-dimensional model of 01005 capacitor with 0.4x0.2x0.2 mm package size will be developed in Ansys FLUENT simulation. The two-way interaction between continuous phase and discrete phase of the model are solved using volume of fluid (VOF) and discrete phase model (DPM). The multiphase-DPM will be used to simulate the interaction between discrete phase nanoparticles and continuous phase fluid flow. Conventional reflow process will undergo a reflow temperature profiles based on real reflow process. The reflow wetting process of SAC305 occurs within the range of temperatures between 217ºC-239ºC as depicted in Fig. 1. It should be noted that the wetting process of SAC305 happens at the wetting zone. In this multiphase-DPM coupling, three different types of nanoparticle are being doped in the SAC305 namely titanium dioxide (TiO_2), nickle oxide (NiO) and Iron (III) oxide (Fe_2O_3) at 0.01, 0.05 and 0.15 weight percentages. These nanoparticles were mixed with the SAC 305 molten solder prior to the soldering process. The properties of the different nanoparticles are shown in Table 2.

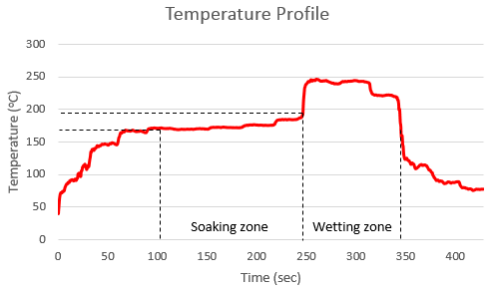

Fig. 1. Thermal profile.

Table 2 Properties of titanium dioxide (TiO_2), nickle oxide (NiO) and Iron (III) oxide (Fe_2O_3). Haslinda *et al.* (2017)

Properties	TiO_2	NiO	Fe_2O_3
Density, p (kg/m$^{3)}$	4250	6810	5240
Specific heat capacity Cp (J kg ºK)	686	603	628
Thermal Conductivity (Wm/K)	8.95	46.02	12.55
Diameter, d (nm)	≈20	≈20	≈20

2.1. Grid Independent Analysis

The most optimum mesh grid resolution generated for the 3D model will be analyzed based on the distribution of the pressure. The lowest grid resolution that managed to obtain the most optimized simulation result will be selected to reduce the computation time required. Table 3 show the pressure based on different grid resolution. From mesh grid independent analysis graph, as in Fig. 2, the most optimized grid resolution is mesh mode number 5 with 21935 number of nodes and 97186 number of cells being used that can compromise between both computational time and accuracy.

Table 3 Grid independent study by depicting the grid resolutions of 0.01 wt.% NiO

Mesh Model	Number of nodes	Number of cells	Gauge Pressure (Pa)	Discretization error (%)
1	15238	70091	5335.62	29.51
2	19199	91201	6771.05	10.54
3	19308	91819	7365.23	2.69
4	20706	96595	7501.54	0.80
5	21935	97186	7569.16	-

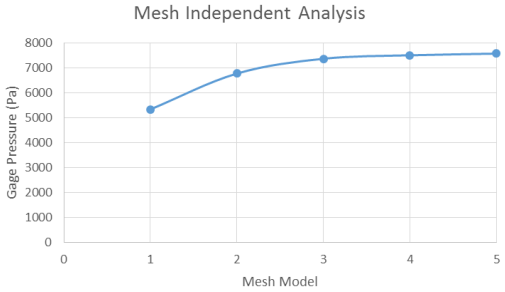

Fig. 2. Mesh independent analysis graph.

2.2. Mesh Generation

The 01005 capacitor being used in this paper is based on real dimensions of 0.4 x 0.2 x 0.2mm and is mounted on an organic solder that is capable of preserving the surface finish of the printed circuit board (FR4-PCB) with thickness of 2.0mm. Fig. 3(a) shows the mesh of the mounted 01005 capacitor on FR4-PCB and (b) meshing model of 01005 capacitor.

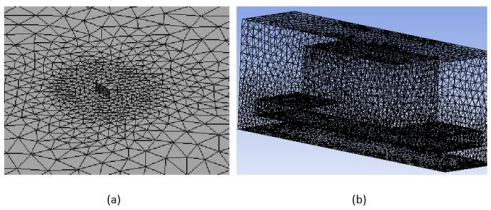

Fig. 3. Meshing grid (a) 01005 capacitor mounted on the PCB and (b) 01005 capacitor.

2.3. Mathematical Modelling

The governing equations for the continuous phase flow of the molten solder SAC305 are solved using continuity, momentum and energy equations. The Navier Stokes formulations will be solved simultaneously during the flow advancement as given by Eqs. (1), (2) and (3).

Continuity equation:

$$\frac{\partial \rho}{\partial t} + \nabla.(\rho u) = 0 \tag{1}$$

Energy equation:

$$\rho C_P \left(\frac{\partial T}{\partial t} + u \nabla T \right) = \nabla (k \nabla T) + \Phi \tag{2}$$

Momentum equation:

$$\frac{\partial}{\partial t}(\rho u)+\nabla.(\rho u u)=-\nabla P+\nabla.\bar{\bar{\tau}}+\rho g \tag{3}$$

where, ρ is the density, u is the velocity, $\bar{\bar{\tau}}$ is the shear stress and gravity g = -9.81 m/s. The momentum transfer term exerted by discrete particle will be, F. The discrete modelled in volume cell will not affect the content of the cell. This is due to the uncoupling with the particle volume that turns to be less accurate at higher volume fraction of solid particles (Xu *et al.* 2014).

The flow advancement of the molten solder is solved using interaction of two Eulerian phases in which the primary phase is set as air and secondary phase is SAC305. Fig. 4 shows the interaction between both phases. The surface tension of SAC305 acting in air is set with σ = 0.54 n/m (Fima *et al.*, 2012).

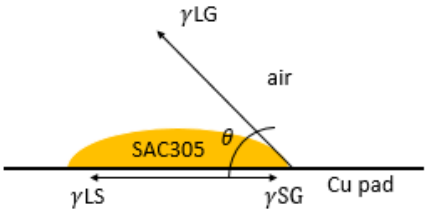

Fig. 4. Surface tension of SAC305 acting on Cu pad and air.

The Young's equation for the formulation of surface tension coefficient acting on the surface for SAC305 can be represented as:

γSG = γ LS + γ LG cos θ

γLG – surface tension of the SAC305-air boundary

γSG – surface tension of the Cu pad-air boundary

γLS – surface tension of the SAC305-Cu pad boundary

θ – contact angle

The multiphase model of the free flow between air and SAC305 is tracked using volume of fluid (VOF) method. This VOF method will distinguish both Eulerian phases within the range of $0 < f < 1$, in which f is the fluid volume fraction. The governing equation can be defined as in Eq. (4). The presence of SAC305 molten solder is denoted as 1 in which it is initially patched at the PCB to mimic the real soldering process.

$$\frac{\partial \rho}{\partial t}f+u\nabla f=0 \tag{4}$$

Discrete phase model (DPM) is modelled on a Lagrangian coordinate to allow accurate tracking of the nanoparticles. DPM is used to track the trajectory and the dispersion of the nanoparticles in the molten solder. The interaction of both Eulerian-Lagrangian phases for multiphase DPM model is predicted to solve two-way interaction between the nano-reinforced particles and the lead free solder. The governing equation used to solve the Langragian phase of the nanoparticles is based on particle force balance that involve all of the forces acting on the particles as given in Eqs. (5 - 8).

Particle force balance:

$$\frac{\partial u_p}{\partial t}=F_D\left(u-u_p\right)+g_x\frac{\left(\rho_p-\rho\right)}{\rho_p}+F_x \tag{5}$$

where $F_D(u-u_p)$ is the drag force and can be expressed as in (6):

$$F_D=\frac{18\mu}{\rho_p {d_p}^2}\left(\frac{C_D Re}{24}\right) \tag{6}$$

In which, u is the fluid phase velocity, u_p is the particle velocity in which both are considered to be free flow. The viscosity of the fluid, μ , fluid density, ρ, particle density, ρ_p , where considering $\rho > \rho_p$ and particle diameter is d_p . Additional force acting on the particles is F_x where this force acting due to mass, acceleration and pressure gradient. The F_x acting on each particles expressed in (7) (Haslinda *et al.*, 2017).

$$F_x=\frac{\rho}{\rho_p}u_p\left(\frac{\partial u}{\partial x}\right) \tag{7}$$

Due to the reflow process, the particles will experience change in thermal energy at various temperatures value. Therefore, these change in thermal energy will cause additional force acting on the particle that is based on thermophoresis force as given by (8):

$$F_x=-D_T\frac{1}{m_p T}\left(\frac{\partial T}{\partial x}\right) \tag{8}$$

where the thermophoric coefficient is denoted as D_T.

For the multiphase DPM interaction, an additional force will be exerted due to due particle interactions with the suspended fluid frequently referred to Brownian force. The equation can be expressed as found Eq. (9).

$$F_B=\xi\sqrt{\frac{\pi S_o}{\Delta t}} \tag{9}$$

Here, the ξ is the zero-mean which is a unit-variance-independent Gaussian random numbers. S_o is modelled as:

$$S_o=\frac{216\mu k_B T}{\pi^2 d_p^5\left(\frac{\rho_p}{\rho}\right)^2 C_c} \tag{10}$$

where the Boltzmann constant value is $k_B = 1.38e-16$ erg/K

The motion of the nano size particle takes into account the Cunningham factor C_c which are computed as given in Eq. (11). The motion of the particles at nano-scale level and its free motion particle in molten fluid are captured based on the drag law force, F_D, and free path flow, λ as in (12) and (13).

$$C_c = 1 + \frac{2\lambda}{d_p}\left(1.257 + 0.4e^{-\left(\frac{1.1d_p}{2\lambda}\right)}\right) \quad (11)$$

$$F_D = \frac{18\mu}{\rho_p d_p^2 C_c} \quad (12)$$

where λ is the particle's mean free path,

$$\lambda = \frac{1}{\sqrt{2}\pi n d^2 \rho} \quad (13)$$

with n denoting the particle number density.

The free motion of the particles also considers the lift shear frequently termed as the Saffman's lift force expressed in Eq. (14).

$$F_L = \frac{2K\,\mu^{1/2}\rho d_{ij}}{\rho_p d_p \left(d_{ik} d_{ki}\right)^{1/4}}(u - u_p) \quad (14)$$

where,

K = 2.594, constant

d_{ij} , $d_{ik,}d_{ki}$ = deformation tensor

The trajectory of the movement and dispersion of the nano size particles are associated with the movement of the fluid since the Stoke's number ≈ 10e-9 can be considered to be very small. For this simulation model, due to relatively low Reynolds number of ≈ 10e-11 being applied the forces will tend to act against gravity. Given that the fluid has a high viscosity with low velocity profile, the magnitude of the velocity for the fluid and particles tend to be approximately similar, $u \approx u_p$, and the nanoparticles movement will exert some minor force to the fluid movement.

For the case of Fe_2O_3, it is assumed that the particles are not spheres and are all identical in shape. For the drag law, non-spherical particles have to be computed according to Eq. (15).

$$C_c = \frac{24}{Re}\left(1 + A.Re^B\right) + \frac{C}{1 + \frac{D}{Re}} \quad (15)$$

where, A,B,C, and D are functions of particle sphericity, ψ. The volume and sphericity of the particle can be defined as given in Eqs. (16) and (17),

Volume,

$$V_p = \frac{\pi}{6} d^3 \quad (16)$$

Sphericity,

$$\psi = \frac{\pi}{Sp} d^2 \quad (17)$$

S_p is the surface area of particle

The shape factor, ϕ is the ratio of surface area of a sphere (with the same volume as the given particle) to the surface area of the particle and are defined based on Eqs. (18) and (19).

$$\phi = \frac{\boldsymbol{s'}}{\boldsymbol{S}} \quad (18)$$

$$\phi = \frac{\pi^{\frac{1}{3}}\left(6V_p\right)^{\frac{2}{3}}}{A_p} \quad (19)$$

where, ***s'*** is the surface area of a sphere having the same volume as the particle, ***S*** is the actual surface area of the particle. The Reynolds number, $\boldsymbol{Re_{sph}}$ is computed with the diameter of a sphere having the same volume. The shape factor cannot exceed a value of 1 since the shape is estimated as a cylindrical-likely leading to a computed value of ϕ ≈0.874.

2.4. Boundary Condition

The two-way interaction of the fluid flow and the nanoparticles are will be coupled using DPM and VOF formulations. The wetting of the SAC305 molten solder is doped with nanoparticles that is inert ceramic compound with a diameter of ≈ 20nm. Figure 5 shows the boundary condition for the two-way interaction of the multiphase DPM.

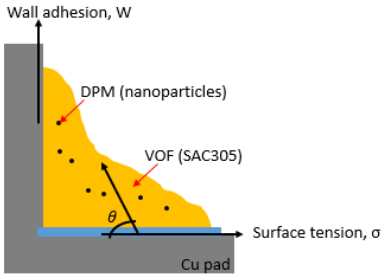

Fig. 5. Schematic diagram of boundary condition.

The dispersion and trajectory of the nanoparticles in discrete phase model has been characterized to satisfy the initial condition, boundary condition, mass flow rate and time step iteration. Initially, 5 mil of SAC305 will be patched into the mesh grid with VOF condition of 1. At different weight percentages of the nanoparticles, the initially doped nanoparticles in a 5 mil volume of SAC305 will experience changes in mass flow rate value during the soldering process. The model exerted surface tension and contact angle due to the interaction between SAC305 and air at 0.54n/m. The wall boundary is set to be no-slip and reflect boundary conditions. The boundary condition can be summarized as follow:

Molten solder:

VOF of fluid= 1,

On wall, $u = v = w = 0$; T=T_{wall} ; $\frac{\partial p}{\partial n} = 0$

On flow front:

Pressure, $P = P_{atm} - \frac{\sigma}{R} = P_{atm} - \frac{2\sigma\cos\theta}{h}$

DPM:

Nanoparticles velocity, $u_p = 0$

2.5. Numerical Solver

The coupling of pressure and velocity is done using Semi-Implicit Method (SIMPLE) algorithm scheme. SIMPLE algorithm scheme is used as multiphase-DPM solver since it enhances the accuracy and tracking capability of the nanoparticles. For the multiphase solder, implicit error <10e-6 is used along with spatial discretization compressive volume fraction. For the tracking of the nanoparticles are set to be continuously interacting with continuous phase at 50000 time steps and at 0.01mm length scale. For all the computations, the under relaxation factor is set to be less than unity and the computed momentum and energy will be solved using second order upwind. The number of time steps and iteration of 0.1x1000 seconds iteration is used to solve both the continuous and the discrete phase.

3. RESULTS AND DISCUSSIONS

3.1. Wetting Time

Wetting time taken for each types of nanoparticles at different weight percentages has been plotted in Fig. 6 that is computed at 20%, 40%, 60% and 80% respectively.

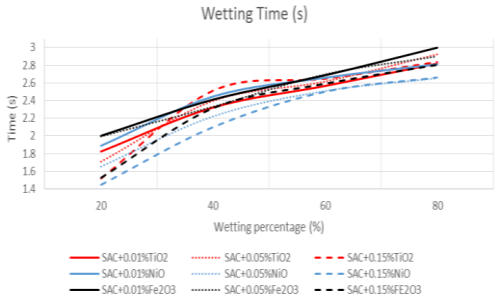

Fig. 6. Plot of wetting time for different types and weight percentages of nanoparticles.

Table 4 Wetting time for different types and weight percentages of nanoparticles

Types of nano-particles	Weight percentage (wt%)	Wetting time (s)
SAC305+ TiO_2	0.01	2.82
	0.05	2.93
	0.15	2.83
SAC305+ NiO	0.01	2.81
	0.05	2.65
	0.15	2.66
SAC305+ Fe_2O_3	0.01	2.99
	0.05	2.90
	0.15	2.80

For each case, it was shown in Table 4 that as the weight percentage of the nanoparticles increases, the time taken for the wetting formation will be reduced. At 80% wetting percentage, SAC305+TiO_2 nanoparticles take 2.82s, 2.93s, and 2.83s for 0.01, 0.05 and 0.15wt%. Conversely, SAC305+ Fe_2O_3 nanoparticles takes longer wetting time with 2.99s at 0.01wt%, 2.90s at 0.05wt%, and 2.80s at 0.15wt%. For the SAC305+ NiO nanoparticles the wetting time taken are 2.81s, 2.65s and 2.66s at weight percentages of nanoparticle for 0.01, 0.05, 0.15 wt% respectively. For the case of 0.15wt% nanoparticles, the wetting time taken for each different types of nanoparticles will differ. SAC305+0.15wt%NiO nanoparticles if shown to have the lowest wetting time taken that is 6.0% lower compared to SAC305+0.15wt%TiO_2 nanoparticles.

For SAC305+0.15wt%Fe_2O_3, the nanoparticles are computed to have the highest wetting time that is 5.65% higher compared to SAC305+0.15wt%TiO_2 nanoparticles. For all cases computed, SAC305+ 0.05wt%NiO nanoparticles is shown to have the lowest time taken for the wetting formation. This will translate to reduction in manufacturing time. The density, shape factor and viscosity of the nanoparticles will influence the flow-ability of the molten solder and the time taken for the wetting. As the weight percentage of the nanoparticle increases, the viscosity of the molten solder changes and consequently leads to an increase in the wetting time. SAC305+ NiO nanoparticles with higher density nanoparticles doped show the least time required for the wetting formation. The density of the nanoparticles causes the time taken for the wetting to be reduced. However, for SAC305+ Fe_2O_3 nanoparticles, the shape factor plays a vital role in influencing the wetting time. Since TiO_2 and NiO are spherical shape, the shape factor is ideally set to 1 while for Fe_2O_3 that is cylindrical in shape will have a shape factor of ≈0.874. This difference in shape factor causes the wetting time for SAC305+ Fe_2O_3 nanoparticles to be highest compared to other cases.

3.2. Flow Front Wetting

The 3D model-view of the distribution of the nanoparticles and the wetted molten solder for different types of nanoparticles at different weight percentages are presented in Fig. 7. From the figure, the trajectory of the nanoparticles at 80% stage are well distributed in the wetted molten solder. Additionally from Fig. 7, the dispersion of the nanoparticles for different types of nanoparticles are observed to be fairly different due to the differences in shape factor and the density of the nanoparticles. From the 3D model-view, it can also be observed that the formation of the wetted molten solder for all case were altered due to the presence of the nanoparticles.

3.3. Nanoparticles Distribution

Figure 8 shows 2-dimensional cross-sectional view of the trajectory for different nanoparticle types at different weight percentages of the nanoparticles. The trajectory of the nanoparticles that are being tracked in the wetted solder were randomly dispersed as can be expected since the Stoke's number for this model at found to be very low. Due to the size of the particles of approximately ≈ 20 nm and the magnitude of the velocity of the nanoparticle, u_p that is approximately similar to the velocity of the fluid, u, in which $u_p \approx u$, the slight difference in the value of velocity between the nanoparticles and the

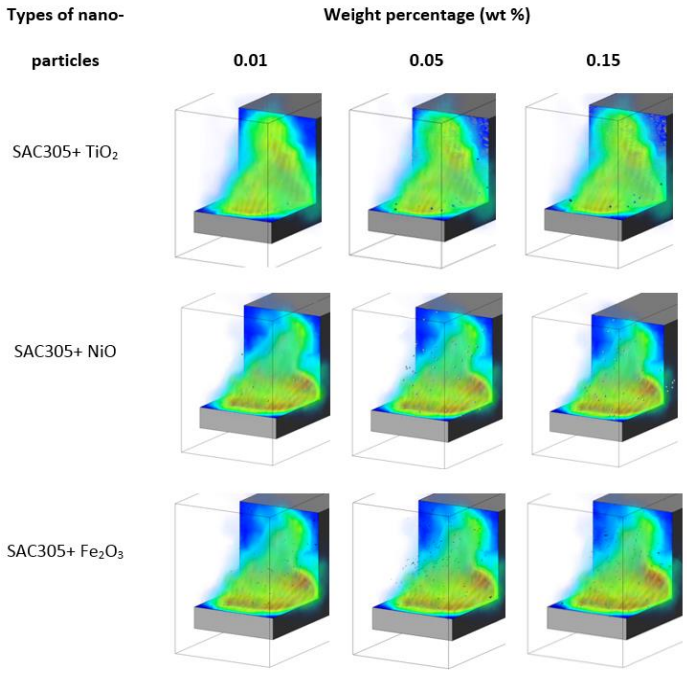

Fig. 7. 3D model-view of wetted SAC305 with nanoparticles.

Table 5 2D model-view of wetted SAC305 with trajectory of nanoparticles

Types of nano-particles	Weight percentage (wt%)	Dimensions (mm)
SAC305+ TiO_2	0.01	0.196
	0.05	0.208
	0.15	0.210
SAC305+ NiO	0.01	0.186
	0.05	0.198
	0.15	0.201
SAC305+ Fe_2O_3	0.01	0.156
	0.05	0.182
	0.15	0.190

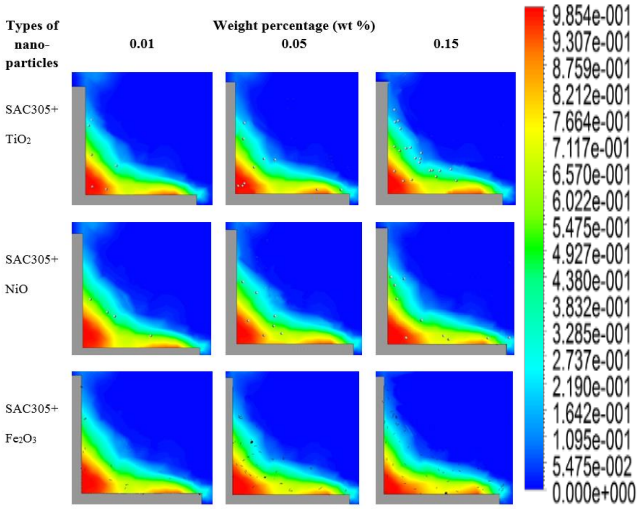

Fig. 8. 2D model-view of wetted SAC305 with trajectory of nanoparticles.

soldering fluid will cause the nanoparticles to exert some forces to the moving fluid. However, this value is relatively small since the change in velocity, momentum and energy can be considered negligible.

From Fig. 8, Fig. 9, Fig. 10 and Fig. 11 for all cases being studied, the trajectory of the nanoparticles in the wetted molten solder were shown to be well dispersed in the molten solder. For 0.15 wt% of the

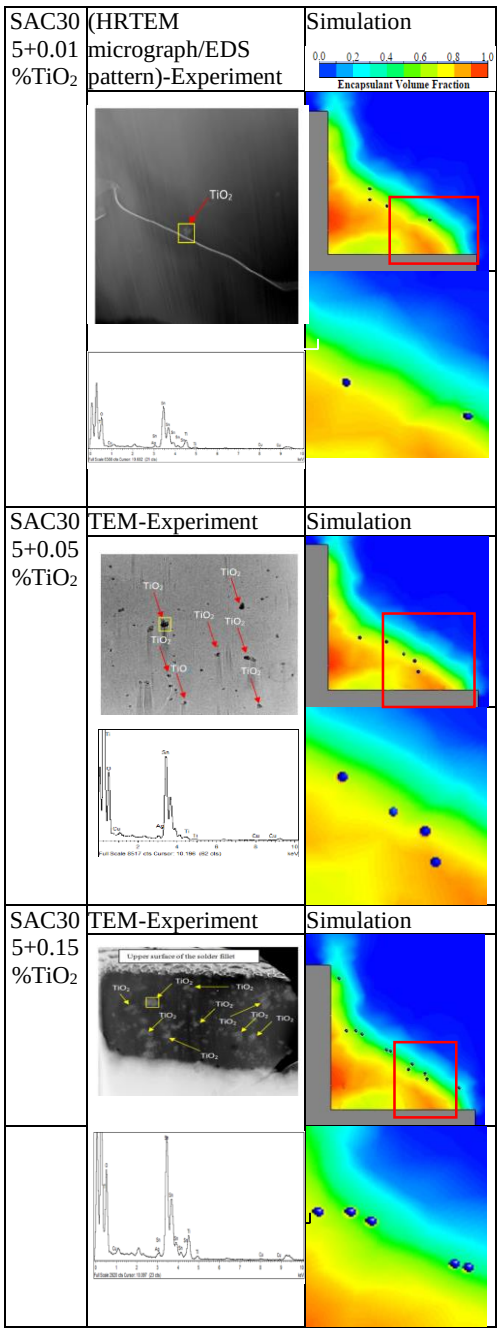

Fig. 9. Comparison of the TiO_2 nanoparticle distribution between simulation and experimental results.

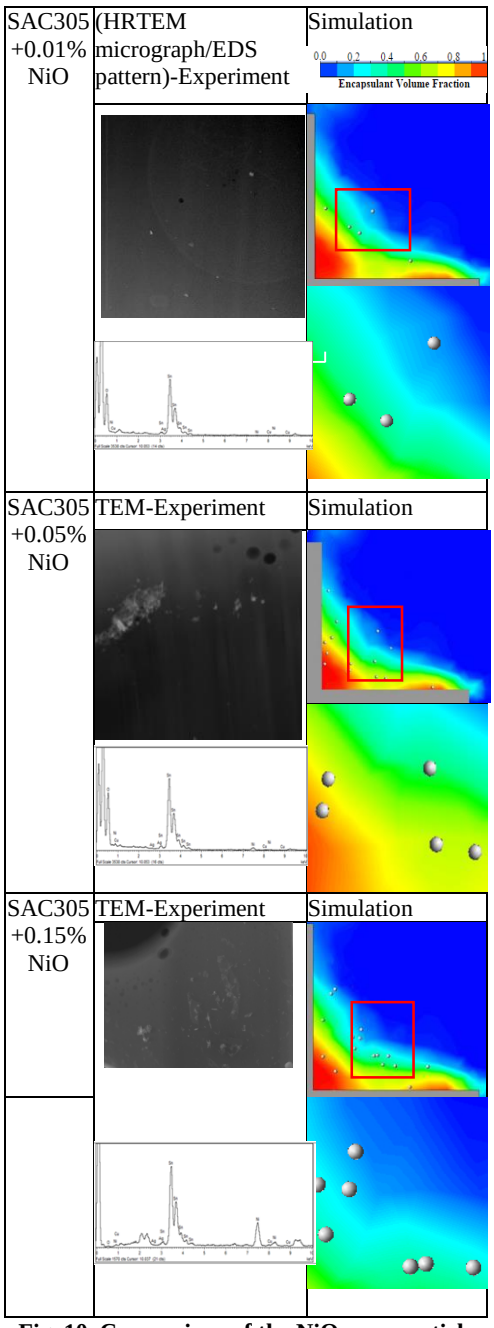

Fig. 10. Comparison of the NiO nanoparticle distribution between simulation and experimental results.

nanoparticles doped in molten solder, the nanoparticles will experience buoyancy effect that is mainly influenced by the density of the nanoparticles. TiO_2 nanoparticles was found to have the highest buoyancy influence effect due to the nanoparticles with much smaller in density compared to NiO nanoparticles. For all cases of nanoparticles at 0.15wt%, the nanoparticles tend to accumulate at the upper region of the wetted molten solder. At 0.15wt% of NiO nanoparticles, the dispersion of the nanoparticles have less buoyancy effect since NiO nanoparticles due to its considerably higher density. In Fig. 11, Fe_2O_3 that is a cylindrical shape nanoparticles have been tracked. The trajectory of the nanoparticles will differ due to the non-sherical shape of the Fe_2O_3 nanoparticles. The numbers of the trajectory nanoparticles tracked in Fe_2O_3 nanoparticles slightly higher compared to the TiO_2 and NiO nanoparticles. As the nanoparticles is being doped in the molten solder, this will improve the strength of the solder joint by hindering the movement of dislocation and pin grain boundaries in the solder matrix which translates in to an increase in the solder deformation resistance (Lee *et al.*, 2008). The increased in reliability of the electronic solder joint will also be improved due to the formation thin IMC layer due to the presence of nanoparticles that will inhibit excessive inter-metallic compound (IMC) growth (Chellvarajoo and Abdullah, 2016).

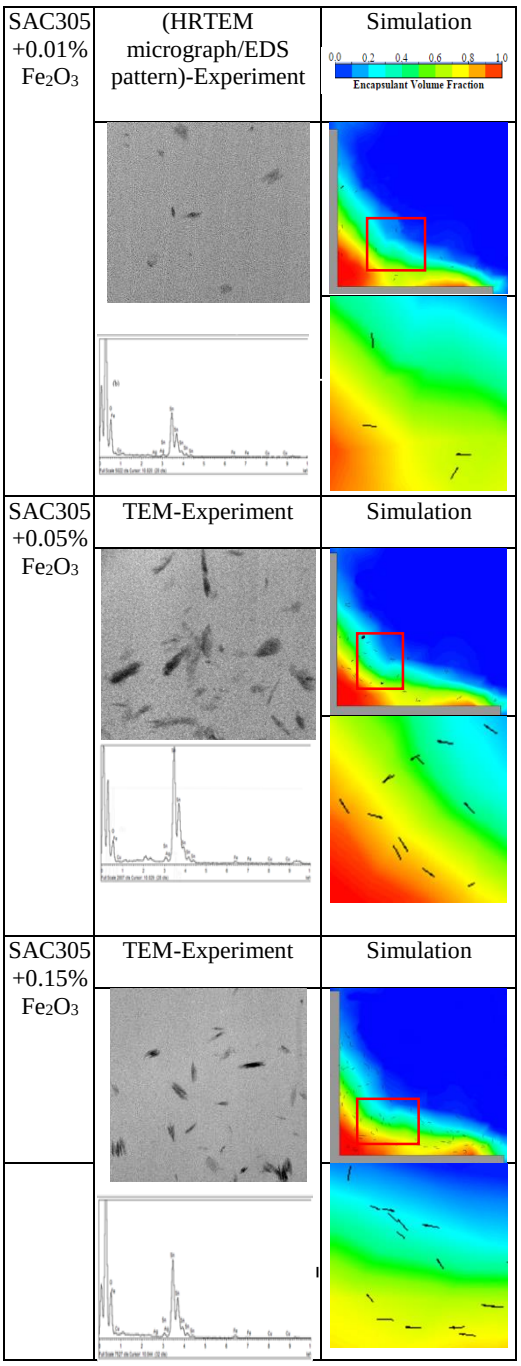

Fig. 11. Comparison of the Fe_2O_3 nanoparticle distribution between simulation and experimental results.

The minimum required fillet height dimension based on IPC-A-610 guideline for a 01005 capacitor is calculated to be with a minimum height of 00.0889mm. The final dimension of the fillet for each cases are summarized in Table 5. From Table 5, the observation and estimated fillet height formation from the numerical result, with different nanoparticles at different weight percentage managed to meet the minimum requirement of the fillet height.

3.4. Velocity Distribution

Probe study to identify the value of velocity and pressure distribution in the wetting formation and trajectory of the nanoparticles distribution will be used in this section. In Fig. 12, few points represented by P- S, near the terminal of the component and T-W, at the base of the PCB board in the simulated model were added to capture the computed pressure and velocity values. The values are then recorded and plotted as in Fig. 13 and Fig. 14.

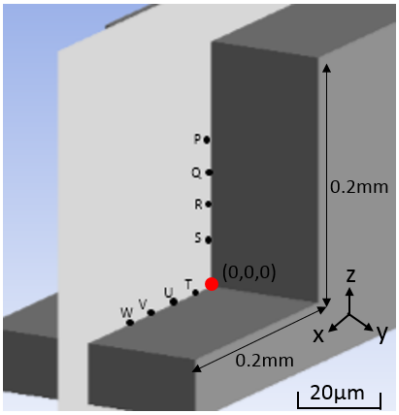

Fig. 12. Specified points near the base metal and the terminal of 01005 capacitor (ultra-fine package).

Based on Fig. 13, for points P-S, TiO_2 nanoparticles show higher velocity distribution compared to NiO and Fe_2O_3 nanoparticles while Fe_2O_3 nanoparticles has the lowest velocity distribution. At points T-W, for all cases, similar velocity distribution were observed. Moreover, at 0.01wt% of the nanoparticles for all different types of nanoparticles has the lowest velocity distribution compared to 0.05wt% and 0.15wt% nanoparticles. The higher the concentration of nanoparticles doped in the molten solder, the higher the velocity distribution of the wetted molten solder. The trend for the velocity distribution for NiO nanoparticles shows a steadier trend for both sides typically at points P-S and points T-W. As previously mentioned, NiO nanoparticles have higher density compared to TiO_2 and Fe_2O_3 nanoparticles hence creating a more uniform and stable velocity distribution. In addition, Fe_2O_3 nanoparticles was found to have the lowest velocity distribution due to the shape factor of the nanoparticle which is cylindrical in shape,

The trajectory of the nanoparticles are also shown to be well dispersed in the molten solder. As previously mentioned in section 3.3, the addition of different types of nanoparticles in this study will promote the formation of thin layer IMC. Due to the presence of the nanoparticles, the growth of the Cu_6Sn_5 IMC grain has been retarded thereby causing the Cu_6Sn_5 IMC to remain in scallop-like shape. Subsequently, Chang *et al.* (2011) study these nanoparticles will reduce the ripening rate of the IMC grains. The IMC layer growth has been refined at thin layer as needed in the electronic packaging to further enhance the reliability of the solder joint.

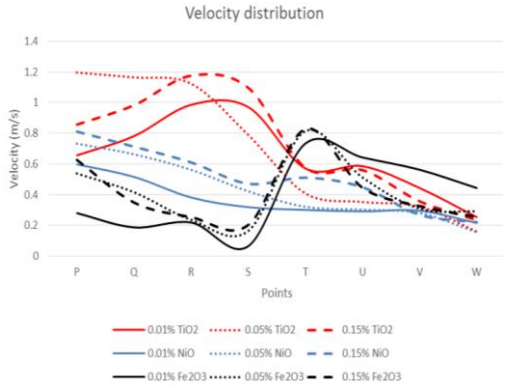

Fig. 13. Graph of velocity distribution of different types of nano-reinforced solder with different weighted percentages nanoparticles.

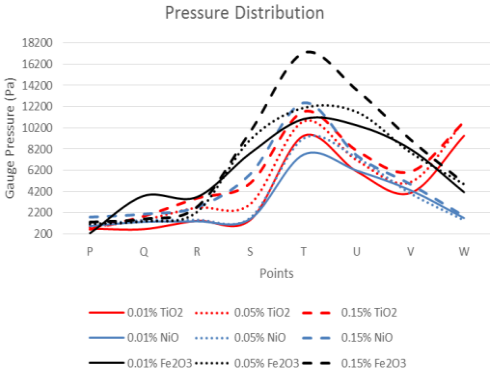

Fig. 14. Graph of pressure distribution of different types of nano-reinforced solder with different weighted percentages nanoparticles.

3.5. Pressure Distribution

Figure 14 shows the pressure distribution for different types of nanoparticle at different weight percentages. For different types of nanoparticle, SAC305 doped with NiO nanoparticles has the highest pressure distribution compared to other nanoparticles. From the trend of the pressure distribution, it was shown that at higher percentage of doped nanoparticles, higher pressure distribution can be observed. From the trend, at points P-S, the pressure distribution is lower compared to the points T-W. According to Fig. 13, with NiO nanoparticles set at 0.15wt% the highest pressure distribution was computed as compared to other cases. Between each types of nanoparticles, 0.15wt% of TiO_2 has a higher pressure compared to 0.01 and 0.05wt% TiO_2. Moreover, 0.15wt% of NiO has a higher pressure distribution compared to 0.01 and 0.05wt% NiO. For nano-reinforced solder with Fe_2O_3 nanoparticles, the pressure distribution increases as the weight percentage of the nanoparticles increases. 0.15wt% Fe_2O_3 has the highest pressure distribution compared to the 0.05wt% Fe_2O_3 and 0.01wt% Fe_2O_3.

From the findings, there exist an irregularity in the pressure distribution throughout the wetting formation. Higher pressure distribution is highly desirable during the wetting process since it tend to inhibits formation of micro-voids. Micro-void formation can cause reduction in the life time and reliability of the electronic component. The addition of nanoparticles in the molten solder has been found to improve the voiding properties in the solder. Based on the computed trajectory of the nanoparticles, it was found that the presence of higher concentration of nanoparticles will increase the domain of higher pressure region henceforth reducing the possibility of micro-void formation as supported by researches done Abas *et al.* (2015) and Ishak *et al.* (2016). From the previous study, it was also found that higher pressure region enables flow front to combine thus further inhibits void formation in solder joint (Ishak *et al.*, 2016). In summary, by doping a controlled amount of nanoparticles in the molten solder can improve the reliability of the solder joint.

4. CONCLUSIONS

Two-way interactions between multiphase VOF and discrete phase model has been applied to study the interaction of SAC305 molten fluid SAC305 with different types of reinforced nanoparticle namely titanium dioxide (TiO_2), nickle oxide (NiO) and Iron (III) oxide (Fe_2O_3) at different weight percentage applied on real scale 01005 capacitor. The wetting formation and trajectory of the nanoparticles in the molten solder were being tracked during this study. According to the results, at higher percentage of nanoparticles, higher wetting time will be required for the wetting formation. From all the computed cases of nano-reinforced solder, SAC305+ 0.05wt% NiO nanoparticles is shown to have the lowest time taken for the wetting formation which can translate into reduction of manufacturing time. The flow-ability of the nano-reinforced solder has been influenced by density and shape factor for the wetting formation. Moreover, the introduction of nanoparticles will refine the size of IMC layer by inhibiting the growth of Cu_6Sn_5 and increased the reliability of the electronic solder joint. Additionally, based on the 2D cross sectional view of the trajectory of the instantaneous nanoparticles, for all case of different %wt and types, it shows that nanoparticles are well dispersed in the molten solder and this will definitely improve the strength of the solder joint. The fillet height of the solder was not affected and managed to meet the minimum height of the fillet for 01005 capacitor. From velocity distribution profile, higher velocity distribution was computed due to high concentration of nanoparticles doped in the molten solder. The flow-ability of molten SAC305 was enhanced at higher pressure that consequently inhibiting the micro-void formation. The pressure distribution also indicates that an increase in the weight percentage of the nanoparticles tend to increase the pressure distribution throughout the wetting process. There are vast amount of interesting analyses that can be improved from the present research work and the results obtained based on the Ansys simulation of the model study. The list of study areas that can be considered and recommended for the future works are given below:

- Extension study of the temperature effect and

thermal stress on the reliability of the solder joint with nanocomposite solder. The study on the temperature and nanoparticles distribution in the solder joint.

- Experiments needed to be performed to determine the time-dependent material properties and is then applied on the numerical model for better simulation results.
- Further study on the fillet formation and fillet height based on the crack propagation of the ultra-fine solder joint at the nanocomposite lead free solder.
- Other numerical simulation study with different software comparison to present study which can determine the accuracy of the simulation results obtained based on different software. This can be done to further verify the result obtained from the current simulation done.

ACKNOWLEDGEMENTS

This research work was partly supported by FRGS grant, FRGS/1/2015/TK03/USM/03/2, Short Term Grant, 60313020 from the Division of Research and Innovation, Universiti Sains Malaysia and Universiti Kebangsaan Malaysia (Research grant–DIP-2014-012)**.** The authors wish to extend their appreciation to Mr. M.Y. Tura and Mr. A. Marzukhi (Jabil Circuit Sdn Bhd) for their technical support.

REFERENCES

Abas, A., M. H. H. Ishak, M. Z. Abdullah, F. C. Ani, S. F. Khor (2015). Lattice Boltzmann method study of bga bump arrangements on void formation. *Microelectronics Reliability* 56, 170-181.

Abas, A., M.S. Haslinda, M. H. H. Ishak, A.S. Nurfatin, M.Z. Abdullah, F. Che Ani (2016). Effect of ILU dispensing types for different solder bump arrangements on CUF encapsulation process. *Microelectronic Engineering* 163, 83-97.

Abas, A., Z.L. Gan, M. H. H. Ishak, M.Z. Abdullah, S.F. Khor (2016).Lattice Boltzmann Method of Different BGA Orientations on I- 34 Type Dispensing Method, *PloS one*, 11(7), e0159357.

Benabou, L., V. Etgens, Q. B. Tao (2016). Finite element analysis of the effect of process-induced voids on the fatigue lifetime of a lead-free solder joint under thermal cycling. *Microelectronics Reliability* 65, 243-254.

Billah, M. M., K. M. Shorowordi and A. Sharif (2014). Effect of micron size Ni particle addition in Sn–8Zn–3Bi lead-free solder alloy on the microstructure, thermal and mechanical properties. *Journal of Alloys and Compounds* 585, 32-39.

Bukat, K. , J. Sitek, M. Koscielski, W. Niedzwiedz, A. Mlozniak, M. Jakubowska, SAC solder paste with carbon nanotubes. Part II: carbon nanotubes' effect on solder joints' mechanical properties and microstructure, *Soldering Surf. Mount Technol* 25 (4) (2013) 195–208.

Bukat, K., J. Sitek, M. Koscielski, M. Jakubowska, M. Sloma, A. Mlozniak, W. Niedzwiedz (2013) SAC 305 solder paste with carbon nanotubes — part I: investigation of the influence of the carbon nanotubes on the SAC solder paste properties, *Soldering Surf. Mount Technol.* 24 (4) 267–279.

Chan, Y. H., M. M. Arafat, A. S. M. A. Haseeb, Effects of reflow on the interfacial characteristicsbetween Zn nanoparticles containing Sn–3.8 Ag–0.7 Cu solder and copper substrate, Soldering Surf. *Mount Technol* 25 (2) (2013) 91–98.

Chang, S. Y., C. C. Jain, T. H. Chuang, L. P. Feng and L. C. Tsao (2011). Effect of addition of TiO_2 nanoparticles on the microstructure, microhardness and interfacial reactions of Sn3.5AgXCu solder. *Materials & Design* 32(10), 4720-4727.

Chellvarajoo, S. and M. Z. Abdullah, (2016). Microstructure and mechanical properties of Pb-free Sn-3.0Ag-0.5Cu solder pastes added with NiO nanoparticles after reflow soldering process. *Materials & Design* 90, 499–507.

Chellvarajoo, S., M. Z. Abdullah and C. Y. Khor (2015). Effects of diamond nanoparticles reinforcement into lead-free Sn-3.0Ag-0.5Cu solder pastes on microstructure and mechanical properties after reflow soldering process. *Materials & Design* 82, 206–215.

Chellvarajoo, S., M. Z. Abdullah and Z. Samsudin (2015). Effects of Fe_2NiO_4 nanoparticles addition into lead free Sn–3.0 Ag–0.5 Cu solder pastes on microstructure and mechanical properties after reflow soldering process. *Materials & Design* 67, 197-208.

Chen, B. L. and G. Y. Li (2004). Influence of Sb on IMC growth in Sn–Ag–Cu–Sb Pb-free solder joints in reflow process. *Thin Solid Films* 462, 395-401.

Chuang, T. H., L. C. Tsao, C. H. Chung, S. Y. Chang, Evolution of Ag3Sn compounds and microhardness of Sn3.5Ag0.5Cu nano-composite solders during different cooling rate and aging, *Materials & Design* 39 (2012) 475–483.

Fallahi, H., M. S. Nurulakmal, A. F. Arezodar and J. Abdullah (2012). Effect of iron and indium on IMC formation and mechanical properties of lead-free solder. *Materials Science and Engineering*: A 553, 22-31.

Fei, C. N., A. Abas, M. H. H. Ishak, M. Z. Abdullah, M. S. Abdul Aziz, (2016). Effect of Thermocapillary Action in the Underfill Encapsulation of Multi-stack Ball Grid Array, *Microelectronics Reliability* 66, 143 – 160.

Fima, P., T. Gancarz, J. Pstrus, K. Bukat and J. Sitek (2012). Thermophysical properties and wetting behavior on Cu of selected SAC alloys. *Soldering & Surface Mount Technology* 24(2), 71-76.

Fouzder, T., I. Shafiq, Y. C. Chan, A. Sharif, W. K. C. Yung, Influence of SrTiO3 nanoparticles on the microstructure and shear strength of Sn–Ag–Cu solder on Au/Ni metallized Cu pads, *Journal of Alloys and Compounds* 509 (2011) 1885–1892.

Gain, A. K. T. Fouzder, Y. C. Chan, W. K. C. Yung (2011). Microstructure, kinetic analysis and hardness of Sn–Ag–Cu–1 wt% nano-ZrO2 composite solder on OSP-Cu pads, *Journal of Alloys and Compounds* 509 (2011) 3319–3325.

Gain, A. K., Y. C. Chan, W. K. C. Yung (2011). Effect of additions of ZrO2 nano-particles on the microstructure and shear strength of Sn–Ag–Cu solder on Au/Ni metallized Cu pads, *Microelectronics Reliability* 51, 2306–2313.

Gain, A. K., Y. C. Chan, W. K. C. Yung (2011). Microstructure, thermal analysis and hardness of a Sn–Ag–Cu–1 wt% nano-TiO2 composite solder on flexible ball grid array substrates, *Microelectronics Reliability* 51, 975–984.

Guo, F. (2007). Composite lead-free electronic solders. Journal of Materials Science: *Materials in Electronics* 18(1-3), 129-145.

Haseeb, A. S. M. A., M. M. Arafat, M. R. Johan (2012). Stability of molybdenum nanoparticles in Sn–3.8Ag–0.7Cu solder during multiple reflow and their influence on interfacial intermetallic compounds, *Materials Characterization* 64 27–35.

Haseeb, A. S. M. A.,T. S. Leng (2011), Effects of Co nanoparticle addition to Sn–3.8Ag–0.7Cu solder on interfacial structure after reflow and ageing, *Intermetallics* 19 (5) 707–712.

Haslinda, M. S., A. Abas, F. C. Ani, A. Jalar, A. A. Saad and M. Z. Abdullah (2017). Discrete phase method particle simulation of ultra-fine package assembly with SAC305-TiO2 nano-reinforced lead free solder at different weighted percentages. *Microelectronics Reliability 79, 336-351.*

Ho, J. and W. Kim (2012). Discrete phase modeling study for particle motion in storm water retention. KSCE *Journal of Civil Engineering* 16(6), 1071-1078.

Ishak, M. H. H., M. Z. Abdullah and A. Abas (2016). Lattice Boltzmann method study of effect three dimensional stacking-chip package layout on micro-void formation during encapsulation process. *Microelectronics Reliability* 65, 205-216.

Kotadia, H. R., P. D. Howes and S. H. Mannan (2014). A review: on the development of low melting temperature Pb-free solders. *Microelectronics Reliability* 54(6), 1253-1273.

Ladani, L. J. and A. Dasgupta (2007). Effect of voids on thermomechanical durability of Pb-free BGA solder joints: Modeling and simulation. *Journal of electronic packaging* 129(3), 273-277.

Lee, A., K. N. Subramanian and J. G. Lee (2005). Development of nanocomposite lead-free electronic solders. *In Advanced Packaging Materials: Processes, Properties and Interfaces, Proceedings.* International Symposium on (pp. 276-281). IEEE.

Lee, J. S., K. M. Chu, R. Patzelt, D. Manessis, A. Ostmann, and D. Y. Jeon (2008). Effects of Co addition in eutectic Sn–3.5 Ag solder on shear strength and microstructural development. *Microelectronic Engineering* 85(7), 1577-1583.

Lee, Y. G., Duh, J. G. (1999). Interfacial morphology and concentration profile in the unleaded solder/Cu joint assembly. *Journal of Materials Science: Materials in Electronics* 10(1), 33-43.

Liu, P., P. Yao, J. Liu (2008). Effect of SiC nanoparticle additions onmicrostructure and microhardness of Sn–Ag–Cu solder alloy, *Journal of Electronic Materials* 37 (6) 874–879.

Liu, Y., H. Fu, F. Sun, H. Zhang, X. Kong and T. Xin (2016). Microstructure and mechanical properties of as-reflowed Sn58Bi composite solder pastes. *Journal of Materials Processing Technology* 238, 290-296.

Lu, L., J. Xu, W. Ge, G. Gao, Y. Jiang, M. Zhao and J. Li (2016). Computer virtual experiment on fluidized beds using a coarse-grained discrete particle method—EMMS-DPM. *Chemical Engineering Science* 155, 314-337.

Rashidi, S., M. Bovand, J. A. Esfahani and G. Ahmadi (2016). Discrete particle model for convective AL_2O_3–water nanofluid around a triangular obstacle. *Applied Thermal Engineering* 100, 39-54.

Salleh, M. M., S. D. McDonald and K. Nogita, (2017). Effects of Ni and TiO 2 additions in as-reflowed and annealed Sn0. 7Cu solders on Cu substrates. *Journal of Materials Processing Technology* 242, 235-245.

Shafiq, I., H. Y. Lau, Y. C. Chan (2013). Effect of trace diamond nanoparticle addition on the interfacial,mechanical, and damping properties of Sn–3.0Ag–0.5Cu solder alloy, *Journal of Electronic Materials* 42 (9) 2835–2847.

Tang, Y., G. Y. Li and Y. C. Pan (2014). Effects of TiO_2 nanoparticles addition on microstructure, microhardness and tensile properties of Sn–3.0 Ag–0.5 Cu–xTiO 2 composite solder. *Materials & Design* 55, 574-582.

Tay, S. L., A. S. M. A. Haseeb, M. R. Johan (2011) Addition of cobalt nanoparticles into Sn–3.8Ag–0.7Cu lead-free solder by paste mixing, Soldering Surf. *Mount Technology* 23 (1) 10–14.

Tay, S. L., A. S. M. A. Haseeb, M. R. Johan, P. R. Munroe, M. Z. Quadir (2013) Influence of Ni nanoparticle on the morphology and growth of interfacial intermetallic compounds between Sn–3.8Ag–0.7Cu lead-free solder and copper substrate, *Intermetallics* 33 8–15.

Thiruvengadam, M., Y. Zheng and J. C. Tien (2016). DPM simulation in an underground entry: Comparison between particle and species models. *International Journal of Mining Science and Technology* 26(3), 487-494.

Tsao, L. C. S. Y. Chang, C. I. Lee, W. H. Sun, C. H. Huang (2010). Effects of nano-Al2O3 additions on microstructure development and hardness of Sn3.5Ag0.5Cu solder, *Materials & Design* 31 4831–4835.

Tsao, L. C., R. W. Wub, T. H. Cheng, K. H. Fan, R. S. Chen (2013) Effects of nano-Al2O3 particles on microstructure and mechanical properties of Sn3.5Ag0.5Cu composite solder ball grid array joints on Sn/Cu pads, *Materials & Design* 50 774–781.

Tsao, L. C., S. Y. Chang (2010). Effects of nano-TiO2 additions on thermal analysis, microstructure and tensile properties of Sn3.5Ag0.25Cu solder, *Materials & Design* 31, 990–993.

Xu, S., Y. C. Chan, K. Zhang, K. C. Yung (2014) Interfacial intermetallic growth and mechanical properties of carbon nanotubes reinforced Sn3.5Ag0.5Cu solder joint under current stressing, *Journal of Alloys and Compounds* 595 92–102.

Yang, L. M., Z. F. Zhang (2013) Effects of Y2O3 nanoparticles on growth behaviors of Cu6Sn5 grains in soldering reaction, *Journal of Electronic Materivals* 42 (12).

Yunus, M., K. Srihari, J. M. Pitarresi and A. Primavera (2003). Effect of voids on the reliability of BGA/CSP solder joints. *Microelectronics Reliability* 43(12), 2077-2086.